The Prp19 U-box Crystal Structure Suggests a Common Dimeric Architecture for a Class of Oligomeric E3 Ubiquitin Ligases[†,‡]

Craig W. Vander Kooi,[§,||] Melanie D. Ohi,[¶] Joshua A. Rosenberg,[#] Michael L. Oldham,[○,§] Marcia E. Newcomer,[○,▽] Kathleen L. Gould,[⊥,#] and Walter J. Chazin*[,§,||,@]

Department of Biochemistry, Center for Structural Biology, Howard Hughes Medical Institute, Department of Cell and Developmental Biology, and Department of Physics, Vanderbilt University, Nashville, Tennessee 37232, Department of Cell Biology, Harvard Medical School, 240 Longwood Avenue, Boston, Massachusetts 02115, and Departments of Biological Sciences and Chemistry, Louisiana State University, Baton Rouge, Louisiana 70803

Received September 5, 2005; Revised Manuscript Received November 1, 2005

ABSTRACT: Prp19 is an essential splicing factor and a member of the U-box family of E3 ubiquitin ligases. Prp19 forms a tetramer via a central coiled-coil domain. Here, we show the U-box domain of Prp19 exists as a dimer within the context of the Prp19 tetramer. A high-resolution structure of the homodimeric state of the Prp19 U-box was determined by X-ray crystallography. Mutation of the U-box dimer interface abrogates U-box dimer formation and is lethal in vivo. The structure of the U-box dimer enables construction of a complete model of Prp19 providing insights into how the tetrameric protein functions as an E3 ligase. Finally, comparison of the Prp19 U-box homodimer with the heterodimeric complex of BRCA1/BARD1 RING-finger domains uncovers a common architecture for a family of oligomeric U-box and RING-finger E3 ubiquitin ligases, which has mechanistic implications for E3 ligase-mediated polyubiquitination and E4 polyubiquitin ligases.

Post-translational modification of target proteins via covalent attachment of ubiquitin and ubiquitin-like modifiers (ubl)[1] is a central regulatory mechanism utilized in many different cellular pathways (*1*, *2*). The most extensively studied mechanism of ubiquitin-mediated signaling involves polyubiquination of substrate proteins leading to target degradation by the 26S proteosome (*3*, *4*). However, the addition of either one or a few ubiquitin molecules has been shown to mediate protein activity, protein−protein interactions, and subcellular localization (*5*−*7*).

Addition of ubiquitin is accomplished via a conserved enzyme cascade consisting of activating (E1), conjugating (E2), and ligating (E3) enzymes (*8*−*10*). There is generally one activating E1 and approximately 20 conjugating E2s. These are complemented by hundreds of E3 ligases, which provide the essential substrate selectivity for modulation of the specific signaling pathways (*10*). Similar cascades (E1, E2, E3) exist for the different ubl pathways such as SUMO, Nedd8/Rub1, and Hub1.

U-box-, RING-finger-, and HECT-domain-containing proteins represent three families of E3 ubiquitin ligases. RING-finger and U-box E3s facilitate the transfer of Ub by precise spatial orientation of the E2 and the substrate rather than binding Ub directly as seen in the HECT family (*11*). The U-box or RING-finger domain serves as the E2 recruitment domain, while another distinct domain, such as leucine-rich repeats or WD40 repeats, serve to recognize and recruit the substrate. RING-finger proteins represent the largest family of E3 ubiquitin ligases. Their structure is characterized by eight conserved zinc-chelating residues that bind two zinc atoms in a cross-braced orientation (*12*, *13*). U-box domain proteins are the most recently identified family of E3 ligases (*14*−*18*). Although the U-box domain is structurally homologous to the RING-finger domain, it lacks the eight canonical zinc-chelating residues found in the RING-finger (*14*, *19*). Instead, the U-box is stabilized through two centers composed of hydrogen bonds and salt bridges (*19*, *20*). Despite this difference, RING-finger and U-box domains share a shallow hydrophobic groove that directly interacts with the E2 (*9*, *19*).

E3 ubiquitin ligases fall into two basic categories: either simple or complex. Simple ligases are composed of a single polypeptide that contains either a RING-finger or U-box domain to recruit the E2 and an additional domain(s), such

[†] This work was supported by NIH Grants RO1GM62112 and RO1GM75156 (W.J.C.), the Howard Hughes Medical Institute (K.L.G.), and NIH Grant No. RO1GM55420 and Louisiana Governor's Biotechnology Initiative (M.E.N). Training grant support was provided by NIH to C.W.V.K. (T32GM08320) and J.A.R. (T32CA09385). M.D.O. is an Agouron Institute Fellow of the Jane Coffin-Childs Foundation.

[‡] The atomic coordinates and structure factors have been deposited in the Protein Data Bank, www.pdb.org (PDB ID code 2BAY).

* To whom correspondence should be addressed at Center for Structural Biology, Vanderbilt University, 5140 BIOSCI/MRBIII, Nashville, TN 37232-8725. Phone: (615) 936-2210. Fax: (615) 936-2211. E-mail: walter.chazin@vanderbilt.edu.

[§] Department of Biochemistry, Vanderbilt University.

[||] Center for Structural Biology, Vanderbilt University.

[⊥] Howard Hughes Medical Institute, Vanderbilt University.

[#] Department of Cell and Developmental Biology, Vanderbilt University.

[@] Department of Physics, Vanderbilt University.

[¶] Department of Cell Biology, Harvard Medical School.

[○] Department of Biological Sciences, Louisiana State University.

[▽] Department of Chemistry, Louisiana State University.

[1] Abbreviations: ubl, ubiquitin-like; RING, really interesting new gene; SCF, Skp1/Cullin/F-box; HECT, homology to E6-AP C-terminus; AU, analytical ultracentrifugation.

10.1021/bi051787e CCC: $33.50
Published on Web 12/08/2005

as WD40 repeats, to interact with a substrate. Complex ligases are either multiprotein or multicopy complexes, both of which require complex quaternary structure to function. Some multiprotein complex ligases, such as the SCF and anaphase promoting complex (APC) ubiquitin ligases, are large assemblies of different proteins that together contain only a single E2 recruitment domain and a single substrate recognition domain. Other complex ligases are oligomeric and thus contain multiple E2 recruitment and/or substrate recognition domains. Indeed, numerous RING-finger- and U-box-containing E3 ubiquitin ligases are known to form higher order homo- and hetero-oligomeric species.

The oligomerization of E3 ligases is often mediated by a known oligomerization domain such as a coiled-coil or helical bundle; however, there are also a number of examples where the RING-finger domain itself is known to contribute to the oligomeric interface (*21*, *22*). While there are only a limited number of structural studies characterizing dimerization of RING-finger and U-box domains, biochemical characterization has revealed that many E3 ligases form specific homo- and heterodimeric species that are mediated by direct RING/RING, RING/U-box, and U-box/U-box interactions (*22*−*25*). Further, a prototypical plant U-box, AtPUB14, has been shown to form U-box-mediated dimers of uncharacterized structure (*20*). While the importance of homo- and hetero-dimeric complexes in ubiquitin ligase signaling is clear, it remains to be determined whether the dimer interfaces between RING-finger and U-box domains are conserved and whether a general mechanism(s) for dimerization exists.

This study provides the first structure of a U-box domain dimer. Combined with previous data, the structure enables the construction of a model of the full-length Prp19 homotetramer. In addition, detailed analysis of this structure combined with previous biochemical analyses strongly implies the existence of a common mode of dimerization for certain U-box and RING-finger domains.

MATERIALS AND METHODS

Protein Expression and Purification. Saccharomyces cerevisiae Prp19 constructs were expressed in *Escherichia coli* as 6×HIS-tag fusion proteins from pET15b. Protein was produced and purified using established protocols for Prp19-(1−73) (*19*). Briefly, proteins were expressed using BL21-(DE3) cells (Novagen) in Luria-Broth (LB). For selenomethionine-labeled protein, protein was expressed using 834(DE3) cells (Novagen) in M9 minimal media supplemented with selenomethionine. Proteins were purified using a Ni^{2+}−nitrilotriacetic acid column (Qiagen) with an imidazole gradient from 25 to 500 mM. The 6×HIS-tag was cleaved by incubation with thrombin (1 U/1 mg protein) for 12 h at 4 °C for U-box constructs and 36 h at 4 °C for Prp19(1−133). Protein was then purified using anion exchange over a MonoQ column (Amersham-Pharmacia) with a gradient of NaCl from 10 to 500 mM.

Strains and Media. S. cerevisiae strains used in this study were grown either in synthetic minimal medium with the appropriate nutritional supplements or yeast extract−peptone−dextrose (*26*). Transformations were performed by the lithium acetate method (*27*). A haploid strain containing a temperature-sensitive copy of *PRP19* (*prp19*−*1*) (KGY1811) was transformed with pRS415 plasmids containing either wild-type *PRP19* or *prp19-L15E*. The ability of *prp19-L15E* to rescue growth at the restrictive temperature was scored by spotting serial dilutions and incubating them at permissive (25 °C) or restrictive (36 °C) temperature for 3 days. The *prp19::HIS3 ura3*−*52 leu2*-Δ*1* haploid strain carrying a *URA3*-selectable vector expressing wild-type *PRP19* was transformed with either *PRP19* cDNA or *prp19-L15E* under control of the *GAL1* promoter in a *LEU2*-based vector. Ura^+-Leu^+ transformants were serially diluted on plates in the presence or absence of 5-flourootic acid and uracil to score the ability of *prp19-L15* to rescue growth of the *prp19*Δ strain after 3 days.

Analytical Ultracentrifugation. Sedimentation velocity experiments were conducted with an Optima XLA (Beckman-Coulter, Fullerton, CA), with a 4-hole An60Ti rotor using double sector cells with charcoal-filled Epon centerpieces (path length 1.2 cm) and quartz windows. The experiments were conducted at 25 °C at a speed of 40,000 rpm and concentration profiles measured at 280 nm. The velocity scans were analyzed with the program Sedfit (version 8.7) (*28*) using 300 scans collected approximately 2 min apart. Size distributions were determined for a confidence level of $p = 0.95$, a resolution of $n = 300$, and sedimentation coefficients between 0.1 and 20 *s*.

Crystallization. Crystals of the U-box domain, Prp19(1−58), were prepared in hanging-drop vapor-diffusion experiments with a 1:1 mixture of protein at 15 mg/mL and 33% poly(ethylene glycol) (PEG) 4000, 75 mM $MgCl_2$, 0.1 M Tris, pH 8.5, and 1 mM DTT at 4 °C. Selenomethionine-labeled protein crystals were obtained in 38% PEG 4000, 75 mM $MgCl_2$, 0.1 M Tris, pH 8.5, and 1 mM DTT at 4 °C. Prior to data collection, crystals were serially transferred to mother liquor containing 5, 10, and 15% ethylene glycol and flash-frozen. Diffraction data statistics are summarized in Table 1.

Crystal Structure Determination. Data were collected at the Center for Advanced Microstructures and Devices (CAMD) using beamline PX. Selenomethionine MAD data were collected to 2.5 Å with wavelength selection based on a fluorescence energy scan. The data were processed using DENZO/SCALEPACK (*29*). SOLVE was used to locate all six (one per subunit) expected selenium sites (*30*). Native crystals of the Prp19 U-box dimer diffracted to 1.5 Å. Phase extension and initial model building were accomplished using RESOLVE (*31*). No averaging of the multiple subunits in the asymmetric unit was employed during refinement. Additional model building and refinement was accomplished using XtalView (*32*) and Refmac5 (*33*). Final refinement statistics are summarized in Table 1. The atomic coordinates and structure factors have been deposited in the PDB (PDB ID code 2BAY).

Dimer interfaces were analyzed using the Protein−Protein interaction server (http://www.biochem.ucl.ac.uk/bsm/PP/server/).

RESULTS

Oligomerization State of the Prp19 U-Box. The U-box-containing protein Prp19 possesses three recognized domains: an N-terminal U-box, a central coiled coil, and a C-terminal WD40 repeat β-propeller domain (Figure 1A).

Table 1: Crystal and Refinement Statistics for the Prp19 U-box Dimer

	Crystal			
		SeMet		
	native	edge	peak	remote
beamline	PDX	PDX		
space group	$P2_12_12_1$	$P2_12_12_1$		
wavelength (Å)	1.381	0.979653	0.979344	0.92526
unit-cell parameters				
a (Å)	49.421	49.038		
b (Å)	57.105	56.558		
c (Å)	122.587	122.420		
unique reflections	52742	22973	23144	23461
completeness (%)	93.3 (85.6)	99.9 (100.0)	99.9 (100.0)	99.8 (100.0)
resolution (Å)	1.50 (1.55−1.50)	2.50 (2.59−2.50)	2.50 (2.59−2.50)	2.50 (2.59−2.50)
R_{merge} (%)	6.3 (42.9)	7.6 (39.8)	7.7 (40.1)	7.0 (34.8)
redundancy	7.5 (6.5)	4.5 (4.2)	4.5 (4.4)	4.2 (4.0)
I/σ (I)	38.7 (3.1)	14.0 (3.2)	13.3 (3.1)	13.4 (3.8)

Refinement Statistics			
resolution limits (Å)	22.93−1.50	Ramachandran	
number of reflections	49928	most favored	91.8
used in refinement		additionally allowed	8.2
number of reflections	2632	generously	0.0
used to compute R_{free}		dissallowed	0.0
R (R_{free})	18.2 (20.4)		
no. protein atoms	2758	rms deviations	
no. solvent molecules	387	bond (Å)	0.012
		angle (deg)	1.5

Recently, we demonstrated using electron microscopy (EM) and analytical ultracentrifugation that Prp19 exists as a tetramer, with the coiled-coil domain serving as the primary oligomerization domain (*34*). The EM studies also revealed that, in the absence of additional binding partners, the Prp19 WD40 repeat domains are flexibly tethered to the tetrameric core of the molecule (*34*). The U-box domain was not directly detectable by EM due to its small size. Thus, the status of the U-box domain in the context of the Prp19 tetramer remained unclear.

To obtain insight into the structure of the U-box within the context of the Prp19 tetramer, a construct was characterized, Prp19(1−133), which contains both the N-terminal U-box and central coiled-coil domain. The oligomerization state of this construct was determined by analytical ultracentrifugation. The major peak (75%) exhibited a sedimentation value (*s*) of 2.7 with a frictional ratio of 1.9. This is consistent with a tetrameric state of 66 kDa (Figure 1B) and reaffirms our previous finding that the coiled-coil domain is both necessary and sufficient for Prp19 tetramerization (*34*). In addition to the tetramer, a small amount of monomer (<10%, $s = 1.1$) and higher order species (∼15%) were detected in the analytical ultracentrifugation analysis (Figure 1B). The frictional ratio indicates an elongated molecule, consistent with the presence of an extended coiled-coil domain linked to the globular U-box (*34*).

CD and NMR spectroscopy were then used to characterize the secondary and tertiary structure of Prp19(1−133), as compared to the intact Prp19 tetramer and the isolated U-box. The minima in the CD spectrum at 208 and 222 nm indicate Prp19(1−133) is a well-folded protein with mainly helical secondary structure (Figure 1C), as expected, based on the previous U-box structure and the predicted coiled-coil region. Analysis of the ^{15}N-^{1}H HSQC NMR spectrum of Prp19(1−133) reveals extensive line broadening with only a few broad resonances discernible (Figure 1D), which is nearly identical to the spectrum of the intact Prp19 tetramer. This result is insightful because it strongly implies that, in the context of the tetrameric coiled-coil domain, the U-box domains do not exist as flexibly tethered independent domains but, rather, Prp19(1−133) tumbles as a single unit. If the U-box domains were flexibly tethered to the core coiled-coil tetramer, narrow signals would be observed in the NMR spectrum corresponding closely to those of the isolated U-box domain, as has been seen, for example, in the small independent RPA32C domain of the ∼50 kDa RPA14/32 complex and the C-terminal domains of the L7/L12 stalk proteins in the intact ribosome (*35*, *36*).

To obtain deeper insight into the state of the U-box in the context of the Prp19 tetramer, we used analytical ultracentrifugation to examine the propensity of the isolated U-box domain to self-associate. This analysis shows that the Prp19 U-box exists in equilibrium between two states, which are assigned to a monomer ($s = 1.4$) and a dimer ($s = 2.1$) in a ratio of 7:3 (Figure 1E) with a frictional ratio of 1.3. Thus, although weak, the U-box does have an intrinsic propensity to dimerize. Importantly, we have observed that the equilibrium is shifted toward the dimer by increasing ionic strength and protein concentration. These results have implications for the U-box, indicating that the propensity to dimerize will be enhanced significantly in the context of intact Prp19 due to the close spatial proximity of pairs of U-boxes on either side of the tetramer (Figure 1F). This can be understood by considering that tethering of the U-box via a short (∼10 residue) linker to the tetrameric coiled-coil domain results in a very high local concentration of U-boxes, which shifts the monomer−dimer equilibrium strongly toward the dimeric state.

To summarize, the EM, AU, CD, and NMR data, taken together, strongly support our contention that the Prp19 U-box exists in a dimeric state in the context of intact Prp19. This conclusion is fully consistent with previous yeast two-

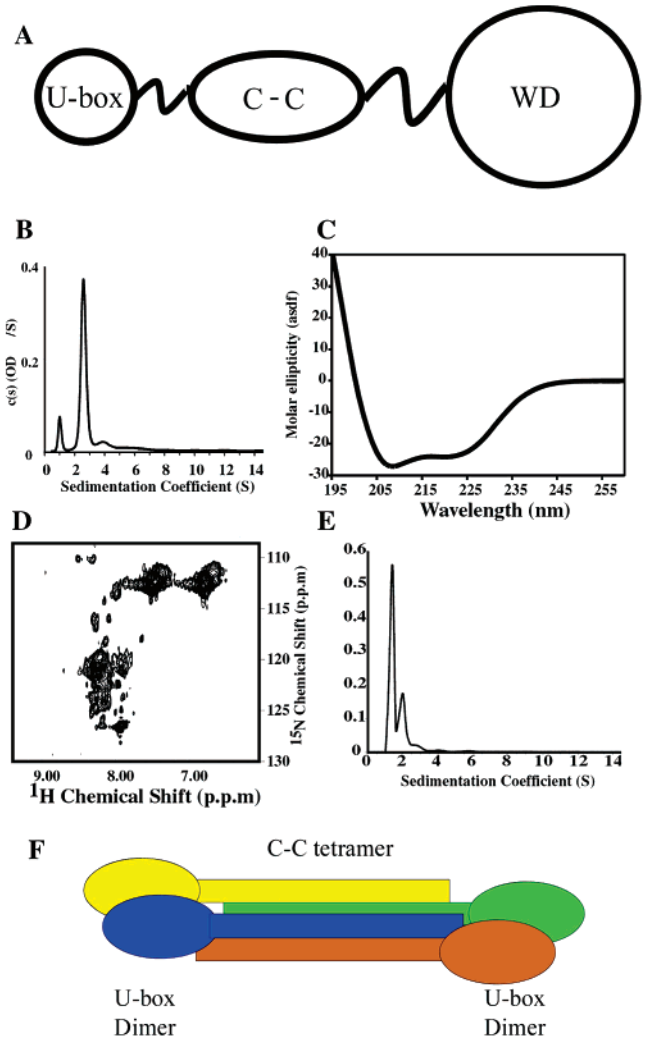

FIGURE 1: The U-box domain of Prp19 exists as a functional dimer. (A) Prp19 contains three domains: an N-terminal U-box, a central tetrameric coiled coil, and a C-terminal WD-40 repeat domain. (B) Analytical ultracetrifugation reveals that the coiled-coil domain drives the formation of a single functional tetramer in the context of a construct containing both U-box and coiled-coil domains. (C) The construct containing U-box and coiled-coil domains is well-structured with primarily helical content. (D) NMR reveals that the U-box domain is integrally connected to Prp19 and not flexibly linked, as is the case for the C-terminal WD40 repeats. (E) The U-box of Prp19 exists in a monomer/dimer equilibrium. (F) A model of the U-box and coiled-coil regions of Prp19 showing the symmetric U-box dimers formed around the coiled-coil tetramer.

hybrid evidence that the U-box domain of Prp19 is involved in protein self-association (*37*).

Crystal Structure of the Prp19 U-Box Dimer. With the objective of producing crystals of the dimeric state of the Prp19 U-box, crystallization trials were set up with a relatively high protein concentration of 15 mg/mL. Crystals were obtained in a relatively rapid manner which diffracted to high resolution. Initial phases were derived from multi-wavelength anomalous diffraction (MAD) experiments using SeMet-substituted protein, and the structure was determined to 1.5 Å, with three dimers in the asymmetric unit (Table 1, Figure 2A). The U-box domain adopts the typical U-box fold, and all copies in the asymmetric unit are superimposable with a backbone rmsd of 0.28 Å (*19*, *20*). The dimer subunits overlay well with the previously reported NMR structure of the Prp19 U-box in the monomeric state (backbone rmsd of 0.94 Å), with all significant differences between the crystal and solution structures at the dimer interface. The major structural difference between the structure of the monomer and the dimer is in the conformation of a loop region immediately adjacent to the third β-strand (residues 53−57), which is involved in critical intermolecular contacts (Figure 2A).

The dimer interface of the Prp19 U-box is formed by residues contributed from the N-terminal loop and the three β-strands. The overall buried surface area is 695 Å^2/subunit with a 69% hydrophobic and 31% hydrophilic character and a high degree of shape complementarity (S_c = 0.75) (*38*). The hydrophobic character of the dimer interface is due to residues Leu15, Ile22, Val51, and Ile53 (Figure 2B,C). Importantly, all four positions are conserved long-chain hydrophobic residues (Val, Ile, Leu) in Prp19 from yeast to man.

Functional Analysis of the Prp19 U-Box Dimer. To assess the role of U-box dimerization in Prp19 function, mutations were made to the residues identified at the dimer interface (Figure 2A), including L15, V51, and I53. To select the best candidate for the more complex biological assays, biophysical analyses of these mutations were performed first to determine how effective these mutations were at disrupting the ability of the Prp19 U-box to self-associate. Not unexpectedly, the most significant effect was from mutation of leucine 15, the hydrophobic residue at the center of the dimer interface. Analytical ultracentrifugation analysis of the L15E mutant provided a single peak with an *s* value of 1.4, indicating it exists exclusively in a monomeric state. The frictional ratio of 1.3 is similar to that observed for the peak of the wild-type monomer. Thus, there is no evidence of the monomer−dimer equilibrium seen for the wild-type protein (Figure 2D, cf. Figure 1E). To ensure that the mutant protein adopts a stable, native-like fold, an ^{15}N-^{1}H HSQC spectrum was acquired for the L15E U-box construct (Figure 2E). The spectrum of the mutant was found to be nearly identical to that of the wild-type U-box, indicating that the structure was not perturbed by the mutation. Consequently, the L15E mutant was selected for analysis of the effect on Prp19 biological activity arising from destabilizing U-box dimerization.

Prp19 is an essential protein and, thus, required for viability. Consequently, the functional significance of Prp19 mutations could be determined *in vivo* by introducing the L15E mutation into the full-length protein. Two complementary approaches were utilized. The first involved assessing the ability of the mutant protein to complement the *prp19* temperature-sensitive allele, *prp19−1*, at the restrictive temperature (Figure 2F, upper panels). The second approach involved complementation of the null allele of *prp19* by a conventional plasmid shuffle approach (Figure 2F, lower panels). The results for L15E in both assays revealed that this single mutation, which disrupts U-box dimerization, is sufficient to compromise cell viability. The origin of this effect is presumably through disruption of the ligase activity of Prp19, or perhaps through destabilization of the NTC complex as observed for the Prp19−1 mutation (*19*). Taken together, the physical and functional effects of dimer interface mutations underscore the physiological relevance of the Prp19 U-box dimer and imply that dimerization of the Prp19 U-box is necessary for its function in vivo.

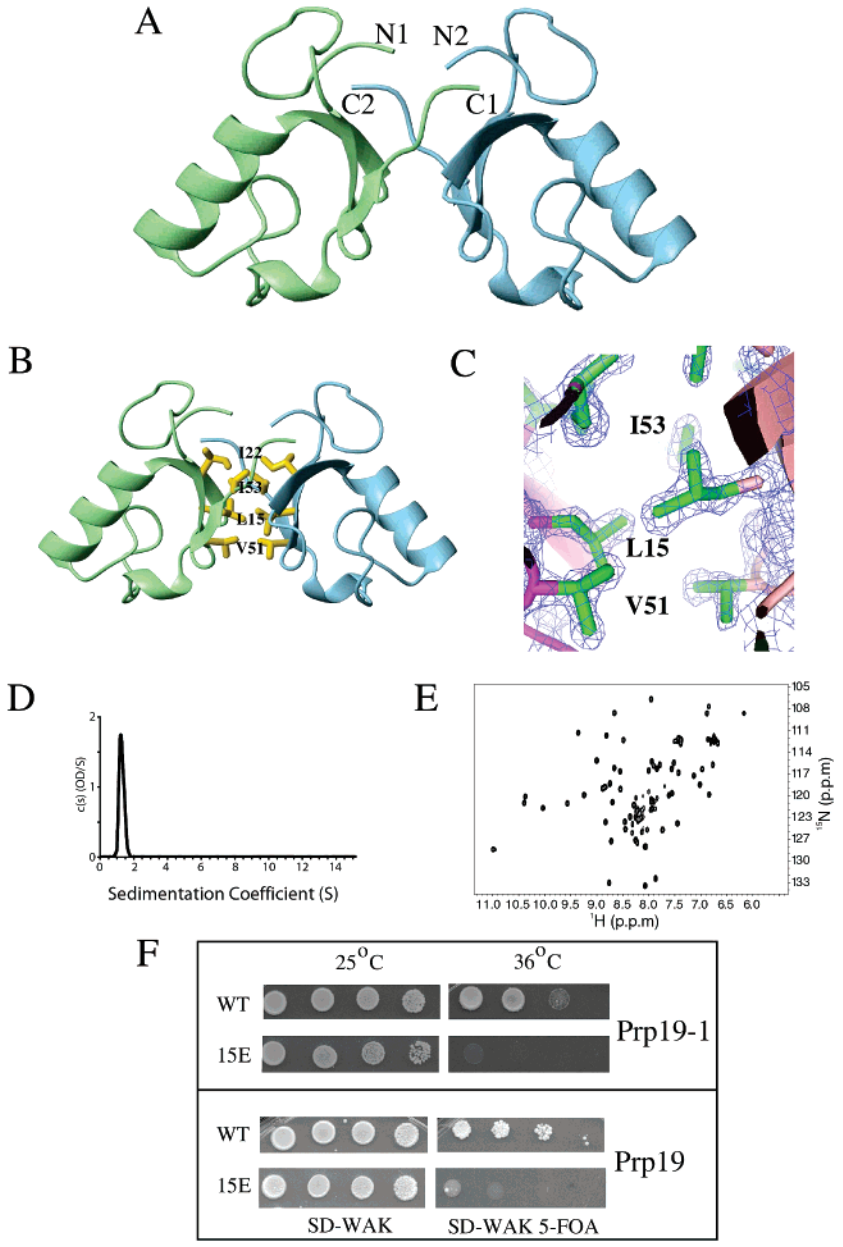

FIGURE 2: Basis for Prp19 dimerization. (A) Ribbon diagram of the Prp19 U-box dimer. Molecular graphics were generated using MOLMOL (*48*). (B) Prp19 contains a central hydrophobic patch at the dimer interface composed of four long-chain hydrophobic residues, shown with a zoom showing the electron density at the dimer interface. (C) Representative $2F_O - F_C$ electron density map of the dimer interface contoured at 2σ (generated with PYMOL; http://www.pymol.org). (D) Mutation of the central hydrophobic L15 to glutamate disrupts the ability of the U-box to dimerize. AU profile of Prp19(1−73) L15E shows only one peak with a sedimentation coeffiecient consistent with the monomeric species. (E) ^{15}N-^{1}H HSQC of the same construct shows excellent line width and chemical shift dispersion, characteristics of a well-folded domain. Additionally, the chemical shifts are virtually superimposable with the wild-type protein (*19*) demonstrating that the L15E mutation causes minimal structural perturbation and adopts a nativelike structure. (F) Mutations to the residues in the dimer interface abrogate Prp19 function *in vivo* either in rescuing a temperature-sensitive strain (upper panel) or rescuing growth for the null allele (lower panel).

Stabilization Centers in the U-Box Domain. As already noted, the binding of two zinc atoms is essential for the stability of the RING-finger domains. The high-resolution crystal structure of the Prp19 U-box provides the first detailed view of the series of hydrogen bonds and salt bridges that serve to stabilize the U-box fold in place of the essential zinc atoms in the RING-finger domains (*19*). Both protein functional groups and tightly bound water molecules are observed in the U-box networks (Figure 3A). Several useful insights have been obtained by comparing to the corresponding zinc-mediated stabilization centers in the crystal structure of the Rag1 RING-finger (Figure 3B) (*39*).

The C-terminal stabilization center in the U-box domain involves four core residues (Ser16, Ser19, Asp38, and Thr41) with the nonconserved Glu43 peripherally involved (Figure 3C). There are no detectable solvent molecules in this network. The overall arrangement is very similar to that of the corresponding zinc-mediated stabilization center seen in RING-finger domains (Figure 3D). In the case of Prp19, Asp38 appears to be central to the interaction network and closely mimics the zinc atom at the center of the RING-finger stabilization center.

A much different picture emerges for the N-terminal stabilization center of the Prp19 U-box, which includes five

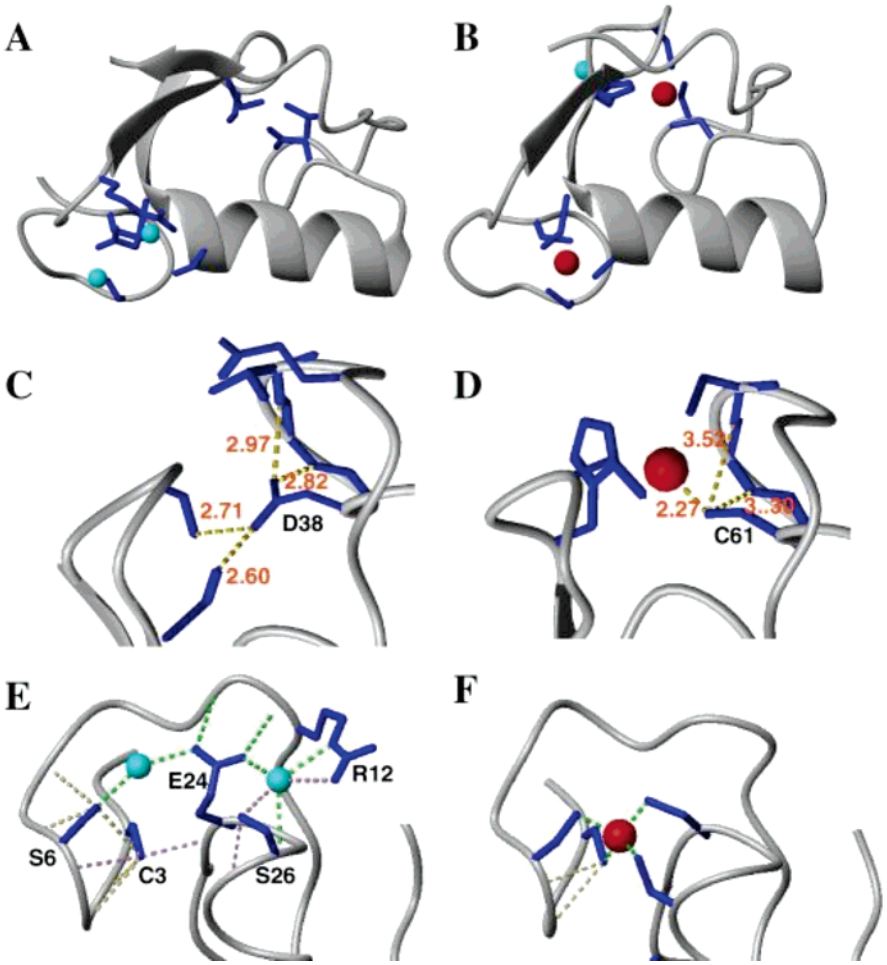

FIGURE 3: Stabilization centers of the U-box domain. (A) U-box domain is stabilized by two networks of hydrogen bonds and salt bridges in Prp19. (B) In contrast, the RING-finger domain of Rag1 (1RMD) is stabilized by chelation of two zinc atoms. (C and D) The C-terminal stabilization center of Prp19 is much more compact and largely recapitulates the organization of the RING-finger center (D), but with Asp38 extended to occupy the position of the central zinc atom. (E) The N-terminal stabilization center of the U-box contains an extended network of inter-residue interactions including many between side chain and main chain amides. Distances between potential hydrogen bond donors and acceptors are color coded: $d < 3.0$ Å as green, $3.0 < d < 3.25$ Å as pink, $3.25 < d < 3.50$ Å as tan. (F) The zinc-mediated RING-finger contains the four zinc−sulfur bonds.

core residues (Cys3, Ser6, Arg12, Glu24, and Ser26) and two high occupancy water molecules (Figure 3E). The backbone trace of this region of Prp19 is virtually superimposable on the RING-finger domain of Rag1 (Figure 3E,F). Despite the remarkable similarity of the backbone conformation, the U-box center differs markedly from that of a RING-finger (Figure 3F). In particular, the residues involved in stabilizing the U-box are more widely distributed than the four zinc-chelating residues in the RING-finger domain, and many more side-chain to backbone amide hydrogen bonds are apparent. In addition, the U-box center includes high-occupancy solvent molecules, something that is not found in the RING-finger structure.

Interestingly, Cys3 and Ser6 in Prp19 are structurally homologous to two of the RING-finger zinc-chelating ligands. Although there is no U-box atom that directly corresponds to the RING-finger zinc atom, Glu24 is located near the center of the extended stabilization site and makes contacts with both solvent molecules and Ser26. The latter is located one residue shifted from the corresponding zinc-chelating residue in the RING-finger domain. This positional shift appears to result in an expansion of the U-box center and the inclusion of the tightly bound water and Arg12. While static pictures of the stabilization centers provide significant insight, analysis of conformational variability within individual molecules and between the different copies in the unit cell reveals these inter-residue interactions are dynamic. For example, differences in the side-chain conformations of Arg12, Glu24, and Ser26 are evident when comparing different molecules in the asymmetric unit.

DISCUSSION

Stabilization of RING-Finger-like Domains. The high resolution structures now available for U-box and RING-finger domains provide a basis for analysis of other related domains. In particular, the comparison of residues now shown to contribute to domain stabilization is highly informative. Consider, for example, the Miz-finger domain, which is related to the U-box and RING-finger domains but is contained in proteins (e.g., the Siz and PIAS families) that function as E3 ligases in SUMOlation as opposed to ubiquitination pathways (*40*). Alignment of the U-box domain of Prp19, the RING-finger domain of Rag1, and several Miz-finger domains provides tantalizing clues to the architecture and structural basis for stabilization of the Miz-finger domain, the structure of which has not been determined. This analysis strongly suggests that the Miz-finger has a unique composition (Figure 4A). The Miz-finger

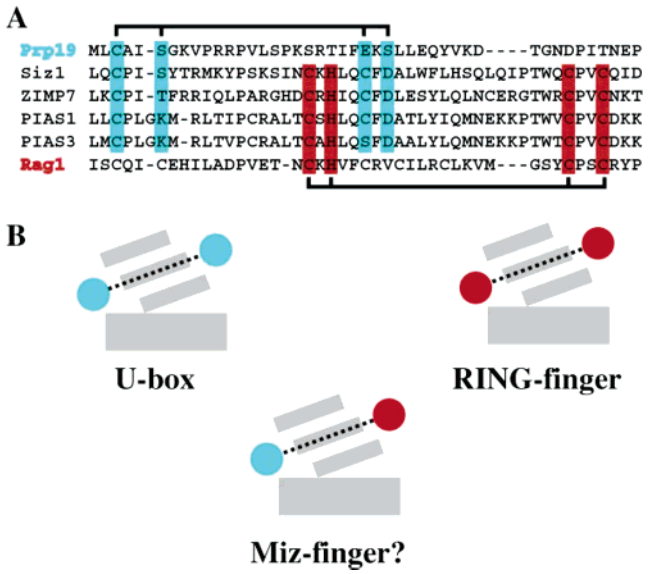

FIGURE 4: Comparison of related E3 ligase domain stabilization. (A) Multiple sequence alignment of Prp19, Rag1, and four human Miz-finger domains. Residues contributing to the N-terminal center of the U-box are highlighted in blue. Residues contributing to the C-terminal center of the RING-finger domain are highlighted in red. (B) Schematic of the cross-braced stabilization of U-box and RING-finger proteins with hydrogen bonding and zinc centers in cyan and red, respectively. Both domains contain a core helix (large rectangle) and three short β-strands (small rectangles). The cross-brace is mediated through the central strand, represented by the dotted line connecting the two stabilization centers. The Miz-finger domain found in related SUMO E3 ligases appears to represent a hybrid of these domains.

domain likely contains a canonical RING-like stabilization center (red) combined with a Prp19 U-box-like stabilization center (aqua) (Figure 4A). Thus, the Miz-finger domain is likely a hybrid U-box/RING-finger domain, with N-terminal stabilization via a network of hydrogen bonds and salt bridges and C-terminal stabilization via zinc chelation (Figure 4B). Since the Miz-finger domains are involved in SUMO-signaling, it is intriguing to consider the biochemical and biological implications of the use of these distinct, yet architecturally similar, domains in parallel cascades. In summary, the addition of the Prp19 U-box to the collection of high-resolution structures of RING-finger domains enhances the ability to predict the molecular architecture of RING-finger/U-box-related domains.

Model of the Prp19 Tetramer. The determination of the structure of the U-box dimer enables construction of a complete model for the intact Prp19 tetramer: a central tetrameric coiled coil, with two U-box dimers and four flexibly attached WD40 repeat domains (Figure 5A). E3 ligases require two essential functional domains: an E2-recruiting domain (e.g., U-box) and a substrate recognition domain (e.g., WD40 repeat domain) (Figure 5B). It is commonly held that the mode of action of the E3 ligase is to bring the E2 and substrate into close proximity, thereby catalyzing the transfer of the activated ubiquitin (*11*, *41*). Utilization of complex quaternary structure for positioning of the E2 and substrate has been proposed to be a common feature of complex E3 ubiquitin ligases such as BRCA1/BARD1 and the multicomponent SCF and APC ligases. For example, the βTrcP1 SCF complex has been proposed to structurally enforce the precise structural positioning of E2

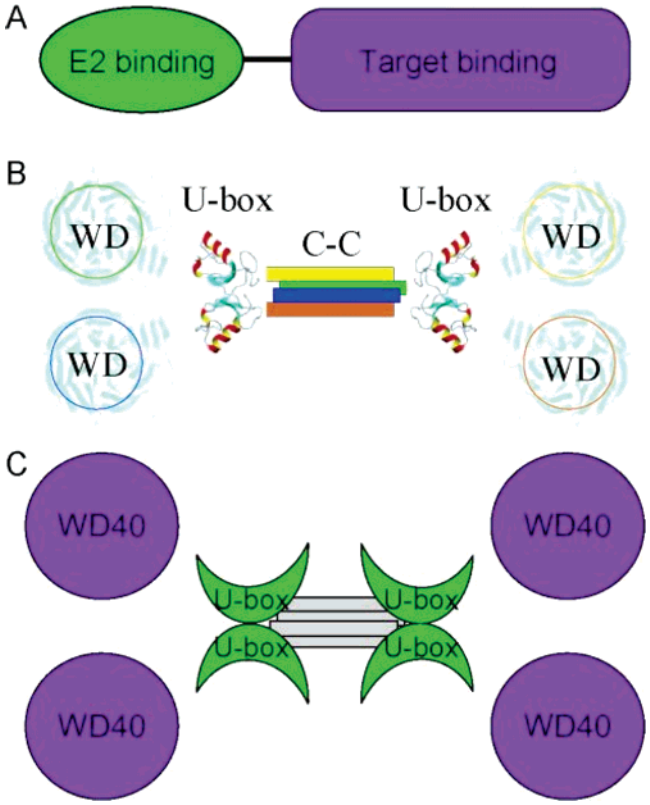

FIGURE 5: Model of the quaternary structure of Prp19. (A) The basic domain structure of an E3 ligase requires E2 and substrate recruitment domains. (B) Prp19 exists as a functional tetramer with dimeric U-box domains and flexibly attached WD40 domains. WD40 repeat domain modeled from Groucho/Tle1 (*49*). (C) The quaternary structure of Prp19 suggests a common architecture for oligomeric E3 ubiquitin ligases that brings the E2 recruitment domain into close proximity with a substrate recognition domain.

and substrate required for catalysis through the spatial organization of the E2-recruiting RING-finger and the substrate-recruiting WD40 repeats (*11*). In any single Prp19 polypeptide chain (protomer), the U-box and WD40 repeat domains are spatially remote. The model of the quaternary structure of Prp19 reveals the U-box domain from one Prp19 protomer is in fact in close proximity to a WD40 repeat domain from one of the other protomers (Figure 5C). It is likely that the molecular scaffold created by the Prp19 tetrameric architecture is important for orienting the E2-recruiting U-box dimer with respect to both WD40 repeats and also to other members of the NTC splicing complex (Figure 5C). Clearly, further structural analysis of Prp19 in complex with substrate and its E2 is required to elucidate the mechanism of action and extent of coordination of the oligomer subunits.

A General Architecture for Dimerization? While the number of characterized oligomeric E3 ubiquitin ligases continues to grow, it remains to be seen if common architectures are utilized to orient both E2 and substrate-recruiting domains. Does the Prp19 U-box dimer reveal a common architecture for orienting and positioning the E2-recruiting domain in an E3 ligase? Dimerization through RING-finger domains in E3 ligases has been examined in two previous studies of Rag1 (*39*) and BRCA1/BARD1 (*21*). Comparison of the topology of Prp19 (Figure 6A) with BRCA1 (Figure 6B) and Rag1 (Figure 6C) is instructive. The Prp19 U-box and BRCA1 RING-finger dimers have

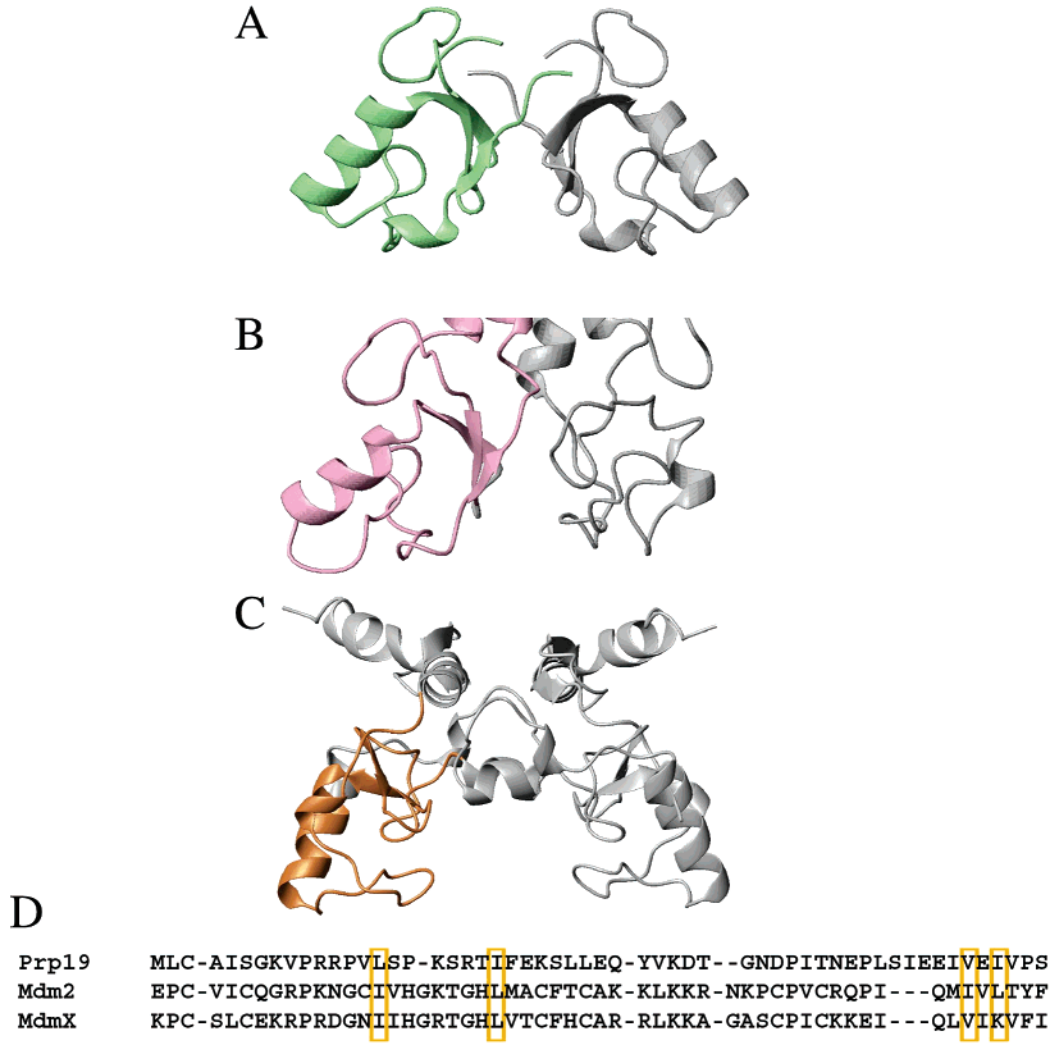

FIGURE 6: The Prp19 dimer as a general model for oligomeric E3 ligases. Comparison of the dimerization interfaces of (A) Prp19, (B) BRCA1/BARD1 (1JM7), and (C) Rag1 (1RMD), respectively, show different characterized dimerization interfaces. The U-box or RING-finger dimerization interface appears structurally conserved between Prp19 and BRCA1. (D) Multiple sequence alignment of dimeric RING-finger domains of Mdm2 and MdmX with Prp19. The four hydrophobic residues at the Prp19 dimer interface are highlighted.

conserved overall topologies with a similar interface (Figure 6A,B). In both cases, the dimer interface is formed by the face of the three β-strands and additional residues from the N-terminus. Importantly, for BRCA1/BARD1, the dimer interface encompasses residues N- and C-terminal to the RING-finger, which come together to form a four-helix bundle. The formation of the stable four-helix bundle provides the driving force for dimerization, which in turn results in steric constraints that orient the two RING-fingers. Thus, we believe the four-helix bundle in BRCA1/BARD1 serves in a role similar to the four-helix coiled coil in the Prp19 tetramer. In the case of the Rag1 homodimer, a helix from each subunit contributes to the dimer interface, which orients the RING-finger domains in-trans with a separation of ~15−20 Å. In all three cases, oligomerization positions the two U-box or RING-fingers in a very similar relative orientation. Thus, it appears there is a common overall architecture positioning the E2-recruiting domains in these U-box/RING-finger oligomeric E3 ligases.

If our hypothesis is correct, this architecture should be present in a range of oligomeric E3 ligases. One such E3 ligase is Mdm2, an important regulator of p53 that belongs to the RING-finger family of E3 ligases that has been shown to form RING-finger-mediated homodimers and also heterodimers with MdmX (*22*, *42*). In fact, there are striking similarities between Mdm2, MdmX, and Prp19 with respect to conservation of the hydrophobic residues critical for formation of the U-box dimer interface (Figure 6C): Mdm2 contains four long-chain hydrophobic residues in these positions and in MdmX three of the four positions are also hydrophobic residues. Thus, it is quite likely that Mdm2 and MdmX utilize a similar dimerization interface and overall architecture as that found in Prp19.

Functional Implications of U-Box/RING-Finger Dimerization. Many essential RING-finger and U-box domain proteins including Mdm2, MdmX, PML, Parkin, Ufd2, and CHIP have been shown to form complex oligomeric E3 ligases (*22*−*25*, *43*). Consequently, it is highly relevant to consider the possible functional implications of the dimeric state of U-box/RING-finger domains. The potential for recruitment of multiple E2 enzymes carrying activated ubiquitin molecules is clearly very important. Prp19 has two identical E2-binding surfaces on opposite sides of the tetramer, and the U-box dimer structure revealed that they are distinct from the dimer interface and therefore both accessible (*9*, *19*). Heterodimerization may offer a means

for functional specificity, enabling the recruitment of two different E2 enzymes. Indeed, BRCA1 has been shown to selectively recruit its E2, Ubc5, in the context of the BRCA1/BARD1 heterodimer (*44*). The ability to recruit multiple and/or different E2 enzymes may play a role in differentiating the type of ubiquitin-like modifications catalyzed by multifunctional E3 ligases. Mdm2, for instance, has been shown to function in either ubiquitin-mediated signaling through recruitment of Ubc5 or in NEDD8 signaling through recruitment of Ubc12 (*45*). In addition, the ability to recruit more than one E2 to the site of ubiquitination may provide a means for the efficient formation of polyubiquitin chains or for the formation of specific branched ubiquitin chains. For example, Ufd2 and CHIP, both U-box domain proteins, can function independently in catalyzing the addition of short ubiquitin chains to UNC-45, whereas the hetero-oligomer is able to rapidly and efficiently polyubiquitinate this substrate (*43*). Thus, the recruitment of multiple E2 enzymes may be critical for the E4 ligase activity observed for Ufd2 (*43*, *46*, *47*).

CONCLUSIONS

The structure and characterization of the U-box dimer shows that oligomerization has important implications for Prp19 function. The organization of Prp19, like other complex ubiquitin ligase families, appears to be finely tuned to orient and align the E2 enzyme and substrate for efficient ubiquitin transfer. Because multiple E2/substrate recruitment modules exist in the Prp19 tetramer, a second consequence of Prp19's complex oligomeric architecture is the potential to couple targeting of substrates. Either positive coupling, where two or more substrates are coordinately targeted, or negative coupling, where either one or another target is selectively or alternately targeted, can be envisioned. While further experiments are required to test and refine these ideas, the potential for control through oligomerization provides an interesting alternative means for directly regulating the ubiquitination of substrates. Investigations along these lines should provide important new insights into the physical basis for the activity of oligomeric E3 family ubiquitin ligases.

ACKNOWLEDGMENT

We thank Drs. Beth Vander Kooi, Joel Harp, Chris Rife, and Thomas Walz, for valuable advice and technical expertise, and Dr. Henry Bellamy for help in data collection.

REFERENCES

1. Schwartz, D. C., and Hochstrasser, M. (2003) A superfamily of protein tags: ubiquitin, SUMO and related modifiers, *Trends Biochem. Sci. 28*, 321−328.
2. Huang, D. T., Walden, H., Duda, D., and Schulman, B. A. (2004) Ubiquitin-like protein activation, *Oncogene 23*, 1958−1971.
3. Hochstrasser, M. (1992) Ubiquitin and intracellular protein degradation, *Curr. Opin. Cell Biol. 4*, 1024−1031.
4. Thrower, J. S., Hoffman, L., Rechsteiner, M., and Pickart, C. M. (2000) Recognition of the polyubiquitin proteolytic signal, *EMBO J. 19*, 94−102.
5. Pickart, C. M. (2001) Ubiquitin enters the new millennium, *Mol. Cell 8*, 499−504.
6. Aguilar, R. C., and Wendland, B. (2003) Ubiquitin: not just for proteasomes anymore, *Curr. Opin. Cell Biol. 15*, 184−190.
7. Haglund, K., Di Fiore, P. P., and Dikic, I. (2003) Distinct monoubiquitin signals in receptor endocytosis, *Trends Biochem. Sci. 28*, 598−603.
8. Walden, H., Podgorski, M. S., and Schulman, B. A. (2003) Insights into the ubiquitin transfer cascade from the structure of the activating enzyme for NEDD8, *Nature 422*, 330−334.
9. Zheng, N., Wang, P., Jeffrey, P. D., and Pavletich, N. P. (2000) Structure of a c-Cbl-UbcH7 complex: RING domain function in ubiquitin-protein ligases, *Cell 102*, 533−539.
10. Pickart, C. M. (2001) Mechanisms underlying ubiquitination, *Annu. Rev. Biochem. 70*, 503−533.
11. Wu, G., Xu, G., Schulman, B. A., Jeffrey, P. D., Harper, J. W., and Pavletich, N. P. (2003) Structure of a beta-TrCP1-Skp1-beta-catenin complex: destruction motif binding and lysine specificity of the SCF(beta-TrCP1) ubiquitin ligase, *Mol. Cell 11*, 1445−1456.
12. Freemont, P. S. (2000) RING for destruction?, *Curr. Biol. 10*, R84−87.
13. Joazeiro, C. A., and Weissman, A. M. (2000) RING finger proteins: mediators of ubiquitin ligase activity, *Cell 102*, 549−552.
14. Aravind, L., and Koonin, E. V. (2000) The U box is a modified RING finger−a common domain in ubiquitination, *Curr. Biol. 10*, R132−134.
15. Hatakeyama, S., Yada, M., Matsumoto, M., Ishida, N., and Nakayama, K. I. (2001) U box proteins as a new family of ubiquitin-protein ligases, *J. Biol. Chem. 276*, 33111−33120.
16. Patterson, C. (2002) A new gun in town: the U box is a ubiquitin ligase domain, *Sci. STKE 2002*, PE4.
17. Cyr, D. M., Hohfeld, J., and Patterson, C. (2002) Protein quality control: U-box-containing E3 ubiquitin ligases join the fold, *Trends Biochem. Sci. 27*, 368−375.
18. Hatakeyama, S., and Nakayama, K. I. (2003) U-box proteins as a new family of ubiquitin ligases, *Biochem. Biophys. Res. Commun. 302*, 635−645.
19. Ohi, M. D., Vander Kooi, C. W., Rosenberg, J. A., Chazin, W. J., and Gould, K. L. (2003) Structural insights into the U-box, a domain associated with multi-ubiquitination, *Nat. Struct. Biol. 10*, 250−255.
20. Andersen, P., Kragelund, B. B., Olsen, A. N., Larsen, F. H., Chua, N. H., Poulsen, F. M., and Skriver, K. (2004) Structure and biochemical function of a prototypical arabidopsis U-box domain, *J. Biol. Chem. 279*, 40053−40061.
21. Brzovic, P. S., Rajagopal, P., Hoyt, D. W., King, M. C., and Klevit, R. E. (2001) Structure of a BRCA1-BARD1 heterodimeric RING-RING complex, *Nat. Struct. Biol. 8*, 833−837.
22. Tanimura, S., Ohtsuka, S., Mitsui, K., Shirouzu, K., Yoshimura, A., and Ohtsubo, M. (1999) MDM2 interacts with MDMX through their RING finger domains, *FEBS Lett. 447*, 5−9.
23. Wei, X., Yu, Z. K., Ramalingam, A., Grossman, S. R., Yu, J. H., Bloch, D. B., and Maki, C. G. (2003) Physical and functional interactions between PML and MDM2, *J. Biol. Chem. 278*, 29288−29297.
24. Imai, Y., Soda, M., Hatakeyama, S., Akagi, T., Hashikawa, T., Nakayama, K. I., and Takahashi, R. (2002) CHIP is associated with Parkin, a gene responsible for familial Parkinson's disease, and enhances its ubiquitin ligase activity, *Mol. Cell 10*, 55−67.
25. Nikolay, R., Wiederkehr, T., Rist, W., Kramer, G., Mayer, M. P., and Bukau, B. (2004) Dimerization of the human E3 ligase CHIP via a coiled-coil domain is essential for its activity, *J. Biol. Chem. 279*, 2673−2678.
26. Guthrie, C., and Fink, G. R. (1991) *Guide to Yeast Genetics and Molecular Biology*, Academic Press, Inc., San Diego, CA.
27. Gietz, R. D., Schiestl, R. H., Willems, A. R., and Woods, R. A. (1995) Studies on the transformation of intact yeast cells by the LiAc/SS-DNA/PEG procedure, *Yeast 11*, 355−360.
28. Schuck, P. (2000) Size-distribution analysis of macromolecules by sedimentation velocity ultracentrifugation and lamm equation modeling, *Biophys. J. 78*, 1606−1619.
29. Otwinowski, Z., and Minor, W. (1997) Processing of X-ray diffraction data collected in oscillation mode, *Macromol. Crystallogr., Part A, 1997 276*, 307−326.
30. Terwilliger, T. C. (2003) SOLVE and RESOLVE: automated structure solution and density modification, *Methods Enzymol. 374*, 22−37.
31. Terwilliger, T. (2004) SOLVE and RESOLVE: automated structure solution, density modification and model building, *J. Synchrotron Radiat. 11*, 49−52.
32. McRee, D. E. (1999) XtalView/xfit−a versatile program for manipulating atomic coordinates and electron density, *J. Struct. Biol. 125*, 156−165.

33. Murshudov, G. N. (1997) Refinement of macromolecular structures by the maximum-likelihood method, *Acta Crystallogr., Sect. D: Biol. Crystallogr. 53*, 240−255.
34. Ohi, M. D., Vander Kooi, C. W., Rosenberg, J. A., Ren, L., Hirsch, J. P., Chazin, W. J., Walz, T., and Gould, K. L. (2005) Structural and functional analysis of essential pre-mRNA splicing factor Prp19p, *Mol. Cell. Biol. 25*, 451−460.
35. Mer, G., Bochkarev, A., Gupta, R., Bochkareva, E., Frappier, L., Ingles, C. J., Edwards, A. M., and Chazin, W. J. (2000) Structural basis for the recognition of DNA repair proteins UNG2, XPA, and RAD52 by replication factor RPA, *Cell 103*, 449−456.
36. Christodoulou, J., Larsson, G., Fucini, P., Connell, S. R., Pertinhez, T. A., Hanson, C. L., Redfield, C., Nierhaus, K. H., Robinson, C. V., Schleucher, J., and Dobson, C. M. (2004) Heteronuclear NMR investigations of dynamic regions of intact *Escherichia coli* ribosomes, *Proc. Natl. Acad. Sci. U.S.A. 101*, 10949−10954.
37. Revers, L. F., Cardone, J. M., Bonatto, D., Saffi, J., Grey, M., Feldmann, H., Brendel, M., and Henriques, J. A. (2002) Thermoconditional modulation of the pleiotropic sensitivity phenotype by the *Saccharomyces cerevisiae* PRP19 mutant allele pso4−1, *Nucleic Acids Res. 30*, 4993−5003.
38. Lawrence, M. C., and Colman, P. M. (1993) Shape complementarity at protein/protein interfaces, *J. Mol. Biol. 234*, 946−950.
39. Bellon, S. F., Rodgers, K. K., Schatz, D. G., Coleman, J. E., and Steitz, T. A. (1997) Crystal structure of the RAG1 dimerization domain reveals multiple zinc-binding motifs including a novel zinc binuclear cluster, *Nat. Struct. Biol. 4*, 586−591.
40. Hochstrasser, M. (2001) SP-RING for SUMO: new functions bloom for a ubiquitin-like protein, *Cell 107*, 5−8.
41. VanDemark, A. P., and Hill, C. P. (2002) Structural basis of ubiquitylation, *Curr. Opin. Struct. Biol. 12*, 822−830.
42. Sharp, D. A., Kratowicz, S. A., Sank, M. J., and George, D. L. (1999) Stabilization of the MDM2 oncoprotein by interaction with the structurally related MDMX protein, *J. Biol. Chem. 274*, 38189−38196.
43. Hoppe, T., Cassata, G., Barral, J. M., Springer, W., Hutagalung, A. H., Epstein, H. F., and Baumeister, R. (2004) Regulation of the myosin-directed chaperone UNC-45 by a novel E3/E4-multiubiquitylation complex in *C. elegans*, *Cell 118*, 337−349.
44. Brzovic, P. S., Keeffe, J. R., Nishikawa, H., Miyamoto, K., Fox, D., III, Fukuda, M., Ohta, T., and Klevit, R. (2003) Binding and recognition in the assembly of an active BRCA1/BARD1 ubiquitin-ligase complex, *Proc. Natl. Acad. Sci. U.S.A. 100*, 5646−5651.
45. Xirodimas, D. P., Saville, M. K., Bourdon, J. C., Hay, R. T., and Lane, D. P. (2004) Mdm2-mediated NEDD8 conjugation of p53 inhibits its transcriptional activity, *Cell 118*, 83−97.
46. Koegl, M., Hoppe, T., Schlenker, S., Ulrich, H. D., Mayer, T. U., and Jentsch, S. (1999) A novel ubiquitination factor, E4, is involved in multiubiquitin chain assembly, *Cell 96*, 635−644.
47. Richly, H., Rape, M., Braun, S., Rumpf, S., Hoege, C., and Jentsch, S. (2005) A series of ubiquitin binding factors connects CDC48/p97 to substrate multiubiquitylation and proteasomal targeting, *Cell 120*, 73−84.
48. Koradi, R., Billeter, M., and Wuthrich, K. (1996) MOLMOL: a program for display and analysis of macromolecular structures, *J. Mol. Graphics 14*, 51−55.
49. Pickles, L. M., Roe, S. M., Hemingway, E. J., Stifani, S., and Pearl, L. H. (2002) Crystal structure of the C-terminal WD40 repeat domain of the human Groucho/TLE1 transcriptional corepressor, *Structure (London) 10*, 751−761.

BI051787E